Double photoionization of atomic oxygen: Feshbach resonances in the two-electron continuum

T W Gorczyca[1], **C P Ballance**[2], **S T Manson**[3], **D Kilcoyne**[4] **and W C Stolte**[4,5]

[1] Department of Physics, Western Michigan University, Kalamazoo, MI, United States of America
[2] School of Mathematics and Physics, Queen's University Belfast, Belfast, BT7 1NN, Northern Ireland, United Kingdom
[3] Department of Physics and Astronomy, Georgia State University, Atlanta, Georgia, United States of America
[4] Advanced Light Source, Lawrence Berkeley National Laboratory, Berkeley, CA, United States of America
[5] Present Address: Nevada National Security Site, Livermore Operations, Livermore, CA, United States of America

E-mail: gorczyca@wmich.edu

Keywords: double photoionization, oxygen atoms, synchrotron sepctroscopy, R-matrix

Abstract

We describe a joint experimental and theoretical investigation on oxygen double photoionization—the emission of two electrons from atomic oxygen following single photon absorption. High-resolution experimental measurements were performed at the Advanced Light Source, revealing sharp resonance structure superimposed on the more familiar Wannier-like, nearly-linear background. These resonance features are attributed to ionization-plus-excitation Feshbach-resonances embedded in the double ionization continuum, doubly-excited states that lie above the double;-ionization threshold. Such features are absent in the double photoionization cross section of He, or other quasi-two-electron systems, for which the doubly-ionized atomic core remains cannot inert. For a corresponding theoretical analysis, the R-matrix with pseudostates (RMPS) method was invoked by calculating final-state, two-electron resonances-plus-continua wavefunctions and corresponding single-photon absorption cross sections. Overall agreement is found in the direct, background double photoionization cross section. However, the RMPS method, using a small basis due to practical computational limitations, was unable to reproduce quantitatively the smooth background or the sharper resonance features observed in the measurements, showing instead large-scale oscillations about the experimental background, and characteristic pseudoresonance jitter, associated with an insufficient convergence of the pseudostate representation to the true two-electron infinite series of Feshbach resonances embedded in the two-electron continuum. The prominent resonance structure observed highlights the need to consider multiple excitation processes in atoms more complex than He or quasi-two-electron systems.

1. Introduction

Double photoionization of an atom (the ejection of two electrons via the absorption of a single photon) is interesting for a number of reasons. In particular, this process is forbidden by any direct absorption pathway due to the one-body nature of the electron-photon interaction. The existence of a two-electron transition such as double ionization is, thus, only possible owing to multi-body electron-electron correlation effects and serves as a probe of these correlations.. From a more fundamental atomic physics perspective, this process constitutes the quantum-mechanical three-body problem for the final state of a doubly-ionized core ion with two outgoing photoelectrons and, therefore, no analytical solution exists even for He, necessitating a numerical approach for computing the final-state three-body wavefunction.

Helium has been the obvious candidate for most of the double photoionization studies to date—see an earlier comprehensive review [1], and the more recent update [2], for the flavor of the various theoretical and experimental approaches, and the latest status of the helium (γ, 2e) (double photoionization) process. Included

Table 1. RMPS and NIST energies for O, O^+, and O^{2+}.

Atomic State	k^2 (Ryd)		$h\nu$ (eV)	
	RMPS	NIST	RMPS	NIST
O ($2s^2 2p^4[^3P]$)	−1.062	-1.001	0.000	0.000
O^+ ($2s^2 2p^3[^4S]$)	0.000	0.000	13.618	13.618
O^+ ($2s^2 2p^3[^2D]$)	0.270	0.244	17.288	16.943
O^+ ($2s^2 2p^3[^2P]$)	0.421	0.369	19.343	18.636
O^+ ($2s2p^4[^4P]$)	1.121	1.093	28.866	28.488
O^+ ($2s2p^4[^2D]$)	1.565	1.513	34.911	34.198
O^{2+} ($2s^2 2p^2[^3P]$)		2.583		48.721
O^{2+} ($2s^2 2p^2[^1D]$)		2.7661		51.253
O^{2+} ($2s^2 2p^2[^1S]$)		2.975		54.093
O^{2+} ($2s2p^3[^5S]$)		3.131		56.219
O^{2+} ($2s2p^3[^3D]$)		3.676		63.623
O^{2+} ($2s2p^3[^3P]$)		4.972		67.642

in the list of theoretical approaches for treating helium double photoionization is the R-matrix with pseudostates (RMPS) method [3], the most recent calculation [4] showing a cross section in excellent agreement with experiment and other converged calculations. RMPS calculations were also carried out for the quasi-two-electron systems, Be and Mg [5], consisting of two valence electrons outside of a 'frozen' closed shell core, and also achieved converged results. Calculations for Li [6] were also performed in which the remaining 1*s* electron only gives rise to a ^{2S} core. However, to our knowledge, the only calculations carried out for the double photoionization of a more complex atom including resonances has been for the case of Ne [7], in which convergence was not achieved due to an increased computational demand for the open-shell nature of the Ne^{2+} core compared to the inert He^{2+} (or Be^{2+} or Mg^{2+}) core. We note that simpler calculations have been carried out with the resonances omitted, e.g., [8, 9].

Oxygen double photoionization presents an even more formidable task than Ne. Furthermore, oxygen is an important element in astrophysical plasma modeling for a variety of reasons, most notably that it is the third most abundant element in the Universe, with only the structurally simple hydrogen and helium atoms being more abundant. Although oxygen is found predominantly as a diatomic molecular gas in the Earth's atmosphere, it is instead found primarily as a diffuse atomic (as opposed to molecular) gas in the interstellar medium [10]. Atomic oxygen gas has also been experimentally isolated for photoionization measurements [11, 12]. Being a weaker process, double photoionization of atomic oxygen has not been considered as important as single photoionization for astrophysical and atmospheric data, and the only experimental data for double photoionization of oxygen, to our knowledge, consists of the low-resolution results of Angel and Samson [13], and the slightly higher resolution results of He, Moberg, and Samson [14].

The purpose of the present paper is to present recent high-resolution synchrotron measurements for the double photoionization of atomic oxygen, carried out at the Advanced Light Source (ALS), and also present accompanying theoretical calculations using the RMPS method. The rest of the paper is organized as follows. In the next section, we consider in deeper detail the process of double ionization of oxygen leaving a non-inert core. The additional double ionization mechanisms available via the open-shell O^{2+} final-state structure are highlighted, introducing additional resonance mechanisms not possible in He and other quasi-two-electron systems. The specific processes addressed here are first introduced next in section 2. Section 3 presents the experimental analysis from the ALS measurements. Section 4 then describes the RMPS particulars of the present computations, and section 5 compares experimental and theoretical results, followed by a brief summary in section 6.

2. General considerations

The specific mechanisms involved in the double photoionization of oxygen, in a *minimal* configuration description, involve the processes

$$h\nu + \mathrm{O}(1s^2 2s^2 2p^4) \rightarrow \mathrm{O}^{2+}(1s^2 2s^2 2p^2) + 2e^-, \quad (1)$$

$$\rightarrow \mathrm{O}^{2+}(1s^2 2s 2p^3) + 2e^-, \quad (2)$$

$$\rightarrow \mathrm{O}^{2+}(1s^2 2p^4) + 2e^-. \quad (3)$$

We use a minimum basis here so that the calculation does not become intractable. Note that there are twelve $2p^2(^3\mathrm{P}, ^1\mathrm{D}, ^1\mathrm{S})$, $2s2p^3(^{5,3}\mathrm{S}, ^{3,1}\mathrm{P}, ^{3,1}\mathrm{D})$, and $2p^4(^3\mathrm{P}, ^1\mathrm{D}, ^1\mathrm{S})$ ionization thresholds of O^{2+} in LS-coupling, as listed in table 1 for the lower-energy states. Those O^{2+} states lying energetically above the $2p^2(^3\mathrm{P})$ ground-state give rise to photoionized-excited Rydberg resonances, such as the $2s2p^3 nl\epsilon l'$ or the $2s2p^3 nln'l'$ resonance series that is degenerate with, and autoionizes to, the $2s2p^2(^3\mathrm{P})\epsilon l\epsilon' l'$ double ionization continuum.

As an example of such resonances, consider the double photoionization process

$$h\nu + \mathrm{O}(1s^2 2s^2 2p^4) \longrightarrow \mathrm{O}^{+*}(1s^2 2s^2 2p^2(^1\mathrm{D}))nln'l' \quad (4)$$

$$\searrow\downarrow$$

$$\mathrm{O}^{2+}(1s^2 2s^2 2p^2(^3\mathrm{P})) + e^- + e^-. \quad (5)$$

Here a double-excitation resonant pathway is degenerate with, and can autoionize to, the direct double photoionization pathway, leading to a coherent sum of the two transition amplitudes, and a resulting Rydberg series of *Feshbach* resonances [15] superimposed coherently on the structureless background cross section. This is to be contrasted with the case of double photoionization of helium, for which there is no core of atomic electrons left behind and therefore no such Feshbach resonance mechanism. Note also that related processes have been seen in other systems [16–18].

3. Experimental measurements

The experimental technique is identical to that previously described for our measurements on atomic oxygen [11], those of Samson *et al.* [19], and our studies of the photofragmentation of HCl [20] and atomic Cl [21]. The present experimental results were obtained on undulator beamline 10.0.1 at the Advanced Light Source (Lawrence Berkeley National Laboratory, Berkeley, CA, USA), and were an average of several photon energy scans.

The experimental apparatus consists of a mass spectrometer, an interaction cell with suitable lensing for ions, and a detector. The 180° magnetic mass spectrometer has pole faces inclined by 11°, which forces ions to be measured in a cycloidal orbit, and allows the approximately 1 mm wide entrance and exit apertures, which are separated by 152 mm, to be located outside the magnetic field. The electromagnet provides a maximum field of approximately 4000 G at the center of the analyzer gap. The analyzer has a mass resolution of approximately $\mathrm{M}/\Delta\mathrm{M} = 65$, with a theoretical half-width resolution of 1 mass in 130 amu. The transit time for ions to pass through the mass spectrometer is a few microseconds. Photons from the beamline enter the gas cell through an entrance collimator which minimizes scattered electrons, possibly created at the gas-cell entrance aperture, from entering the interaction region. The gas cell has a curved extraction plate which increases the solid angle of acceptance by focusing the ions into the lens system. The Einzel lens system and steering plates focus and direct the ions onto the mass spectrometer entrance slit. In this instance the analyzer and lensing was optimized for mass 16 amu. Ions are detected at the exit slit of the spectrometer with a Dr. Sjuts channel electron multiplier (type KBL-15RS). An analog signal from a convectron vacuum-pressure gauge is recorded simultaneously with the ion signal to monitor target gas pressure. Finally the photon flux after the gas cell, I, is monitored with a Si photodiode.

Calibration of the photon energy is performed by comparison to EELS measurements or known absolute photoabsorption measurements found in the literature. In this case the photon energy was adjusted by correction of the monochromator's grating equation using both the helium $\mathrm{He}(sp,2\,2+)^1P^0$ at 60.147 eV [22], and krypton $3d_{5/2}^{-1}\,5p$ at 91.200 eV [23] transitions. These resonance peaks were measured from first up to third spectral order for the helium transition and up to the fifth spectral order for the krypton transition. This resulted in eight different calibration energies measured over the region of interest. The resulting error in energy calibration on the low energy grating was found to be from +10 meV at 45.6 eV to +42 meV at 60 eV, with a resolution of 15 meV. The photon flux was measured at the back of the experimental system by using a AXUV100 silicon photodiode, with its signal subsequently being corrected for its variation in quantum yield [24] prior to being used for normalization.

Atomic oxygen was produced by passing molecular oxygen through a microwave-driven discharge. A mixture of 20% molecular nitrogen and 80% molecular oxygen, was passed through a glass flow assembly [21]. The flow assembly consisted of a short (12 cm long, 1 cm outer diameter) quartz tube, in which the microwave-driven discharge takes place, and a long (30 cm, 1 cm outer diameter) Pyrex tube, which transports the atoms to the interaction region. To minimize losses due to collisions with the flow tube walls, the quartz tube was coated with phosphorus pentoxide ($\mathrm{P_2O_5}$), and the Pyrex tube was coated with Teflon. An increase of 30% in the

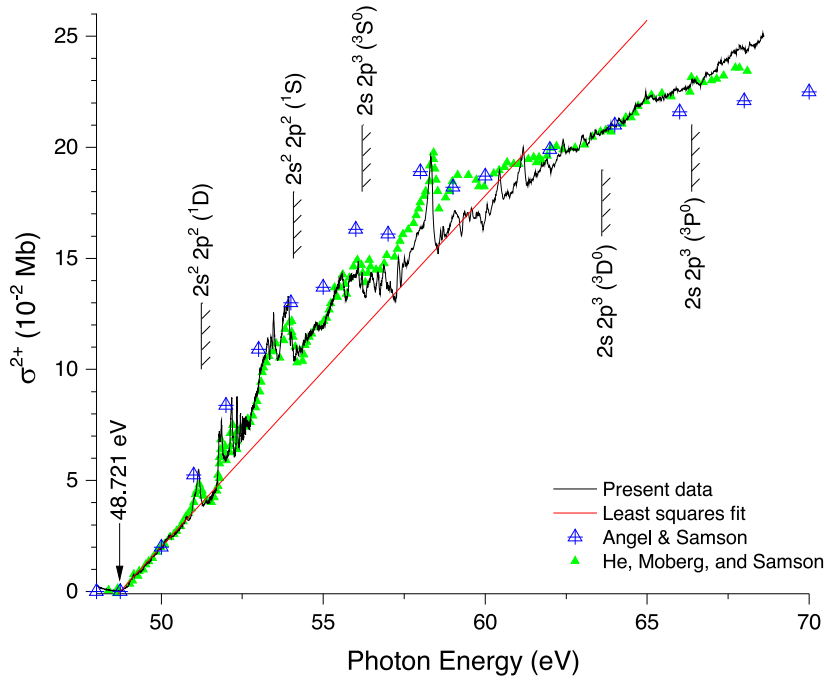

Figure 1. Oxygen double photoionization cross sections, showing present ALS experimental results (black), the earlier Angel and Samson experimental results [13] (blue), and He, Moberg and Samson (green) [14]. The NIST O^{2+*} energies [27], as given by vertical black lines and also listed in table 1, each comprising a threshold for a Rydberg series of photoionized-excited Feshbach resonances in the double ionization continuum. A Wannier-like threshold fit $\sigma^{++} = CE^m$ (red) is also shown with $C = 0.0.014$Mb/eV and $m = 1.056$.

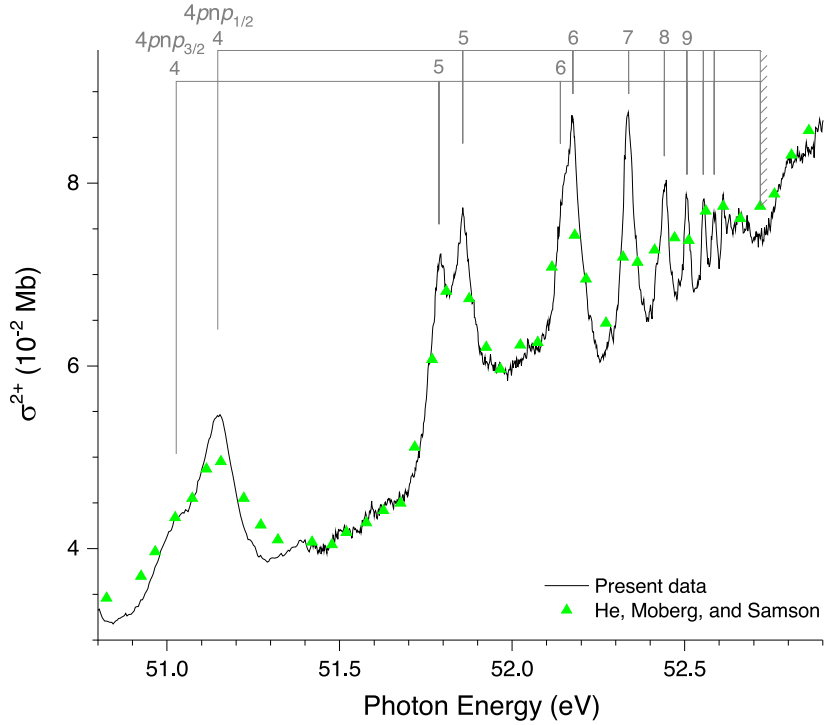

Figure 2. Present experimental results and those of He, Moberg, and Samson [14], showing the autoionization features from doubly excited states converging to the $2s2p^3(^5S^o)4p(^6P^o)$ state.

amount of atomic oxygen transported to the interaction region was seen when using the coated flow tubes rather than clean flow tubes. At the end of the Pyrex flow tube, an additional Pyrex tube (10 cm long, 2.5 cm outer diameter) with a 1.5 mm orifice on one end was used to separate the high pressure discharge region, which was approximately 0.1 Torr, from the low pressure photoionization interaction region (coated with Aerodag G on

Table 2. Present experimental results for the two identified Rydberg series resulting from doubly excited states converging to the $2s2p^3(^5S^o)4p(^6P^o)$ state. N is principal quantum number μ is the quantum defect and $n^* = n - \mu$.

		Present results			He *et al* [14]		
Identification	n	n^*	μ	Photon Energy (eV)	n^*	μ	Photon Energy (eV)
$2s2p^3(^5S^0)4p4p_{3/2}$	4	2.836	1.164	51.041 ± 0.014			
$2s2p^3(^5S^0)4p4p_{1/2}$	4	2.942	1.058	51.161 ± 0.014	2.939	1.061	51.15
$2s2p^3(^5S^0)4p5p_{3/2}$	5	3.823	1.177	51.803 ± 0.015			
$2s2p^3(^5S^0)4p5p_{1/2}$	5	3.973	1.026	51.857 ± 0.015	3.933	1.067	51.85
$2s2p^3(^5S^0)4p6p_{3/2}$	6	4.849	1.151	52.155 ± 0.015			
$2s2p^3(^5S^0)4p6p_{1/2}$	6	5.007	0.993	52.191 ± 0.015	4.941	1.059	52.17
$2s2p^3(^5S^0)4p7p$	7	5.970	1.030	52.352 ± 0.015	(5.940)	(1.060)	(52.34)
$2s2p^3(^5S^0)4p8p$	8	7.000	1.000	52.456 ± 0.015	(6.940)	(1.060)	(62.44)
$2s2p^3(^5S^0)4p9p$	9	7.998	1.002	52.521 ± 0.015			
$2s2p^3(^5S^0)4p10p$	10	9.089	0.911	52.569 ± 0.015			
$2s2p^3(^5S^0)4p11p$	11	10.126	0.874	52.601 ± 0.015			
$2s2p^3(^5S^0)4p(^6P^0)$	∞	series limit		52.734 ± 0.015			52.72 ± 0.03

the high vacuum side to prevent charging). A small mechanical roughing pump is connected between the two Pyrex tubes to allow for a high gas flow rate through the discharge region while maintaining a reasonable chamber pressure, approximately 2×10^{-5} Torr.

The partial-ion yields measured with the discharge *on* as described above include contributions from both ground-state atomic oxygen and molecular O_2, differing as a function of photon energy. Whereas, with the discharge *off* the gas target is composed solely of molecular O_2. Similar to the measurements of He, Moberg, and Samson [14], the present O^{2+} cross sections, shown in figure 1, were normalized to the absolute values of Angel and Samson [13]. These values were chosen because of the careful analysis of all available photoionization and partial photoionization measurements of atomic oxygen by Berkowitz [25, 26]. The previous results of He, Moberg, and Samson were calibrated at 60eV, but the present data, due to our increased resolution shows resonance structure in this area. Therefore, due to the relatively smooth variation in cross section in a region just slightly higher in photon energy, we chose to calibrate at 64 eV. Although these in-between data values were not listed in table 2 of the 1988 publication, we had access to the original data set.

The energy region between 51 and 53 eV is shown in figure 2. It is compared with the results of He, Moberg, and Samson. The most striking difference is the observation of two, overlapping Rydberg series, where one was previously identified. We attribute this to our increased resolution, 15 meV verses 60 meV. The two series, summarized in table 2, are a result from autoionization of doubly excited Rydberg states. The resonances were fit with WinXAS© [28] (Thorsten Ressler, Hamburg, Germany) and its near-edge x-ray-absorption fitting routines. The spectral lines were fit with Voigt functions, with the Gaussian contribution to each peak held at a constant width equal to the measured monochromator resolution, while the Lorentzian portion of the function, which represents the lifetime of the particular state, was allowed to vary. An arctan function was used to represent the ionization threshold, its slope was set to the beamline resolution and its position was allowed to vary after initially setting it to our previous values. All errors in table 2 include standard deviations and beamline calibration errors.

4. Theoretical RMPS methodology

The RMPS method (see [3] for a fairly comprehensive review) has been used for double photoionization of helium dating back to 1995 with the first successful applications by Meyer and Greene [29], followed by further independent developments and applications [30, 31], including the latest converged calculations [4, 31]. The approach has also been used for the quasi-two-electron cases of Be and Mg [5], for the relatively simpler three-electron case of Li [6], and an even more complicated Ne calculation [7]. The latest application of the RMPS method for double photoionization of He was for the case of endohedrally-confined $He@C_{60}$ [4]. In that study, prior to computing the effect of the C_{60} cage, a double photoionization R-matrix calculation for an isolated He atom was performed, using a sufficiently large pseudoorbital basis, and a cross section was produced that showed excellent agreement with experimental and other theoretical results. In the present study, however, due to the orders of magnitude increase in the number of double-continuum basis functions used and the practical computational limitations, only a much smaller basis per double continuum could be used, resulting in an unconverged pseudostate representation for each second continuum orbital, and a noisy cross section.

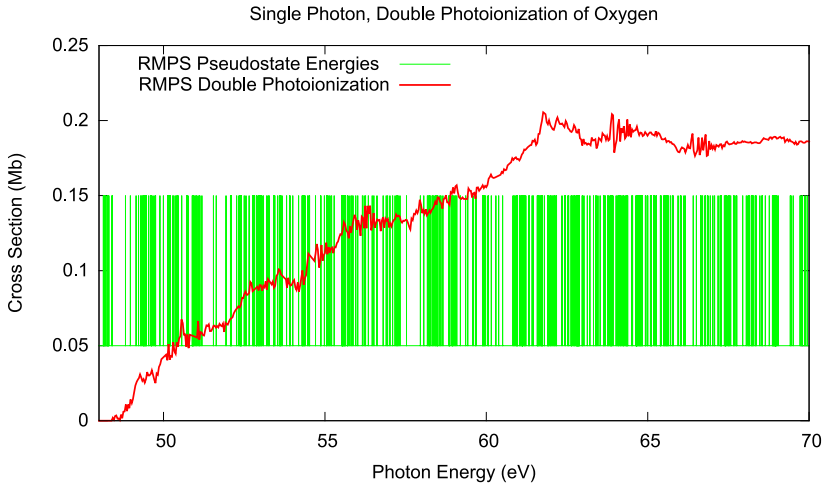

Figure 3. Computed energy positions of the numerous $O^{+*}(1s^2 2s^a 2p^b nl, a+b=4$ target states and pseudostates in the vicinity of the O^{2+} double ionization thresholds, superimposed on the RMPS double photoionization cross section.

From a theoretical standpoint, there is a huge increase in computational requirements for oxygen double photoionization compared to helium. This is because the many-state, structured-core, doubly-ionized states of oxygen that are left behind in the DPI process lead to a much larger atomic basis needed to represent all outgoing channels. An entire basis of two-electron continuum functions is required for each of the many O^{2+} doubly-ionized cores, whereas only one such basis is needed for the two-electrons emitted from the inert He^{2+} core, for instance. The non-inert core also leads to multiple couplings. In He, only an inert He^{2+} core remains after double ionization, and only one LSπ symmetry is possible for each coupled pair of outgoing electrons—e.g., the outgoing two-electron wave $l_1, l_2, L_{12}, s_1 = 1/2, s_2 = 1/2, S_{12}$, with parity $\pi_{1s} = (-1)^{l_1+l_2}$, can only couple to a total symmetry $L = L_{12}, S = S_{12}, \pi = \pi_{12}$. Double photoionization of oxygen, on the other hand, can leave behind several open-shell ionic states, such as the $2p^2(^1D)$ state, for instance, that allows final angular momenta $|L_{12}-2| \leqslant L \leqslant |L_{12}+2|$, adding five additional LSπ symmetries. The ^3P core leads to three L symmetries per L_{12} value and three S symmetries per S_{12} value, adding another nine possible couplings. These two multiplicative factors of the basis size, arising from both the many core doubly-ionized states and also the many couplings of the two-electron continuum to each of the many cores, are then cubed when determining the increased RMPS computational time, leading to a calculation for oxygen that is orders of magnitude larger than the simpler helium case. Clearly, a massively parallel infrastructure is needed, and we have used the Michigan State University High-Performance Computer Center for the RMPS calculations [32].

The particular basis for the RMPS calculations is the following. Physical orbitals, $P_{nl} = \{1s, 2s, 2p\}$, were first generated from a single-configuration Hartree–Fock calculation [33] optimized on the $O^+[1s^2 2s^2 2p^3(^4S)]$ ground state. Next, additional Laguerre *pseudoorbitals* $\overline{P_{nl}}$ were generated, using the atomic AUTOSTRUCTURE code [34], only for $3 \leqslant n \leqslant 10$ and $0 \leqslant l \leqslant 5$, a severely limited size for representing each particular double-electron continuum, of which there are many, hence the small basis (in the recent, converged He calculations [4], pseudoorbitals could be included up through $n \leqslant 30$ to represent the sole double-electron continuum required, and a converged cross section was obtained); the present $n \leqslant 10$ pseudoorbital basis is thus expected to yield unconverged results and therefore exhibit the characteristic, unphysical pseudoresonance jitter, as will be further addressed below.

The physical orbitals P_{nl} and pseudoorbitals $\overline{P_{nl}}$ were then used to construct the so-called N-electron O^+ target configurations describing the $1s^2 2s^a 2p^b, a+b=5$ physical states and $1s^2 2s^c 2p^d\, nl, c+d=4$ pseudostates, thereby providing a discrete representation of the second-electron continuum $\epsilon_2 l'$. The first-electron continuum orbitals $\epsilon_1 l$ are spanned, for each channel energy ϵ_1 and angular momentum l, as $\epsilon_1 l = \sum_{i=1}^{n_{cont}} c_i u_{il}(r)$, where the number of R-matrix continuum orbitals in the present case was chosen to be $n_{cont} = 25$. The usual R-matrix orbital basis, $u_{il}(r)$, is generated for a representative model potential, using Lagrange multipliers to ensure orthogonality between orbitals: $\langle P_{nl}|u_{il}\rangle = \langle \overline{P_{nl}}|u_{il}\rangle = \langle \overline{P_{n'l}}|P_{nl}\rangle = 0$. Such orthogonality constraints simplify the atomic structure calculations since there are no overlap terms to consider in the evaluation of the Hamiltonian matrix [3].

The resulting energies are listed in table 1 for the lower-energy states where it is evident that the use of a small basis leads to reasonable, but not excellent, agreement between theory and experiment [27]. The experimental values for the states of O^{2+} are included in the table without theoretical values because these states appear as

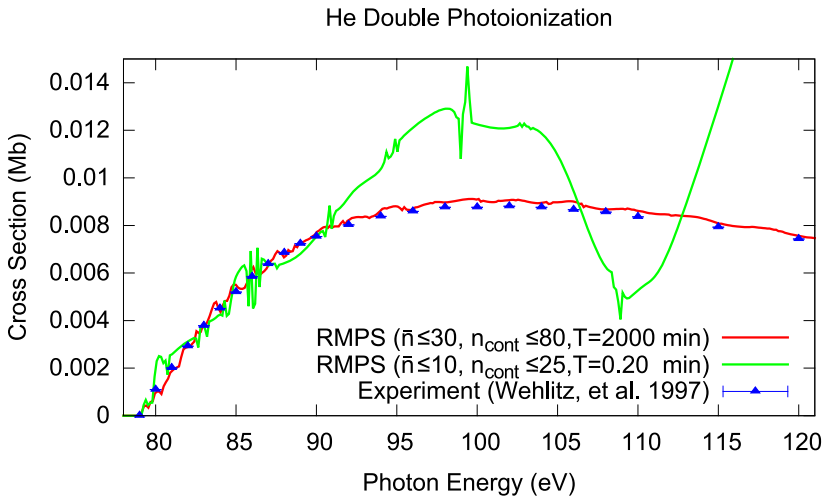

Figure 4. Double photoionization of He, showing the convergence of the RMPS cross section, as the number of pseudoorbitals is increased from $n \leqslant 10$ (green) to $n \leqslant 30$ (red), to the experimental data (blue triangles, [35]).

resonances in the RMPS cross section and are not included in the expansion of the initial and final state wave functions of the photoionization process in the RMPS methodology, as detailed below.

Each continuum orbital is coupled to each of the possible N-electron O^+ configurations to complete the so-called $(N+1)$-electron description. This represents the initial, neutral oxygen atom, the O^+-plus-electron photoexcited resonances, the single-photoionization states, and, importantly, the O^{2+}-plus-two-electron states. The latter include both the desired double photoionization states *and* the photoionization-plus-excitation states that are manifested as Feshbach resonances embedded in the two-electron continuum. To compensate for the enforced orthogonality, an additional $(N+1)$-electron basis is also included, giving additional $1s^2 2s^2 2p^6$, $1s^2 2s^a 2p^b nl$, $a + b = 5$ and $1s^2 2s^a 2p^b nln'l'$, $a + b = 4$ configurations.

In order to compute a double ionization cross section within the RMPS method, the usual single photoionization-excitation cross sections are first computed to each excited pseudostate of O^+ (e.g., $h\nu + 2p^4 \rightarrow 2p^2 nl\epsilon_1 l$), and for all those pseudostates with relative energies exceeding the ionization potential of O^{2+}. The approximation involved is that the second liberated continuum electron e_2^- is discretized via a pseudoorbital representation, so that the double photoionization process can be interpreted as a sum over all partial cross sections to pseudostates that lie energetically above the O^{2+} threshold:

$$\sigma^{++} = \sum_i \sigma_i (E_i > IP). \tag{6}$$

By using the above procedure, the RMPS double photoionization cross section was calculated and is presented in figure 3. Also shown are the O^+ pseudostate thresholds generated from the same RMPS calculation. The pseudostate energy density gives a sense of how well the second electron continuum orbital is represented by an expansion of pseudoorbitals. Of course, the final pseudostates plotted correspond to pseudoorbitals nl with several different angular momenta l and/or couplings to the O^{2+} core, so the actual density per continuum orbital representation is much less than the total pseudostate energy density shown. In fact, since it is known that there are only 8 pseudoorbitals per continuum ($3 \leqslant n \leqslant 10$) spanning this region, the density must be only about 8 states per 20 eV. However, since the total cross section is given as a sum over all $n_i l_i\ \epsilon_i l_{i'}$ states, and some averaging of oscillation occurs from each pseudostate contribution to the total cross section, the total pseudostate density still reveals a sense of how smoothly the introduction of each new threshold approximates the true continuum.

A characteristic feature of RMPS cross sections for double ionization is the unphysical jitter and oscillations associated with the discretized representation of the second continuum. This jitter is reduced as the pseudostate density is increased (as with any Fourier expansion). However, a fairly crude basis of orbitals, as we have here ($3 \leqslant n \leqslant 10$), will inevitably result in unconverged, jittery cross sections, as is demonstrated in figure 4. Here the structurally simplest (and least computationally demanding) He case, as implemented in the converged atomic study in earlier work [4], is revisited. The 'converged' calculation used the larger basis $n \leqslant 30$ and $n_{cont} \leqslant 80$, and yields an RMPS cross section that tracks the smooth experimental data [35]. On the other hand, the smaller calculation, using only a $n \leqslant 10$ and $n_{cont} \leqslant 25$ basis, shows much more erratic pseudoresonance jitter as well as slow oscillations of the RMPS background cross section about the smooth experimental background. The

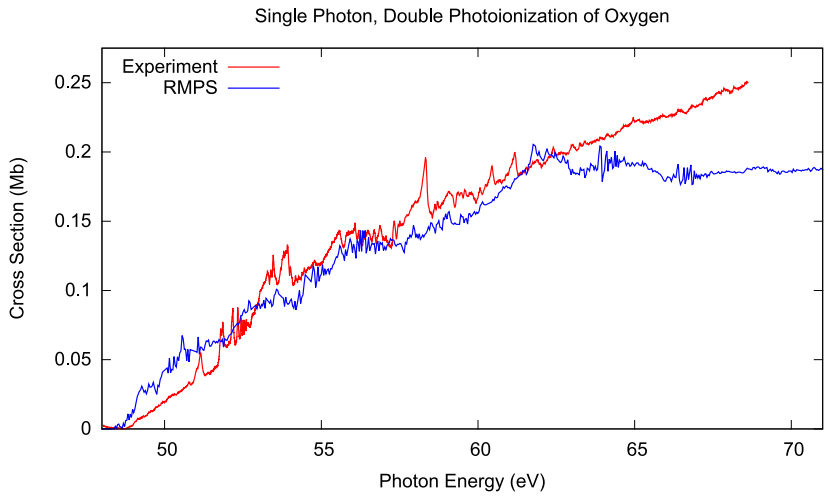

Figure 5. Oxygen double photoionization cross sections: ALS experimental results (red) and theoretical RMPS results (blue).

savings in computational time is significant, as expected. The larger converged case required 2000 minutes of CPU time whereas the smaller, unphysical case required only 0.20 minutes on the same workstation.

The present RMPS calculations for oxygen used the same orbital basis size ($n \leqslant 10$, $n_{cont} \leqslant 25$) as the smaller He case. However, because of the many more resulting pseudostates via multiple core couplings, etc., the total Hamiltonian is much larger, and the computational time is much greater, requiring days to finish on the HPCC massively-parallel machine verses less than a minute for He. Thus we can conclude two things about the RMPS cross sections for oxygen. First, as with the small-basis He cross section shown in figure 4, unphysical jitter and oscillations are expected in our RMPS oxygen cross section, and indeed that behavior, shown in figure 3, is thus explained—it is due to an insufficient pseudoorbital and continuum orbital basis. Second, any attempt to reach similar convergence for oxygen as was achieved for the larger He case (in figure 4) will require about four orders of magnitude more computational effort, an increase from a day to decades with the same machine and an increased number of processors used.

5. Results

In order to analyze the double photoionization cross section most effectively, the experimental results are shown in figure 1, where several interesting features should be noted. First, there is general agreement between the latest and earlier experimental results, although the resolution has now been improved greatly. In fact, the new experiment, similar to the measurements of He, Moberg, and Samson [14], allows a detailed mapping of the threshold region, revealing a nearly-linear cross section at threshold, in accordance with the expected Wannier threshold law [36], that persists for roughly 10 eV above threshold. According to this law, the behavior is linear at threshold if electron-electron correlation is neglected, but once correlation is considered yields a power-law threshold behavior

$$\sigma^{++} = CE^m \tag{7}$$

where

$$m = \frac{1}{4}\left(\sqrt{\frac{100Z-9}{4Z-1}} - 1\right) = 1.055893 \tag{8}$$

for the case of $Z = 2$ here. An experimental least squares fit of the data over a 3 eV range from the double ionization threshold to just below the first resonance arrives at a value of 1.038 ± 0.004. Interestingly, the Wannier cross section is surprisingly good up to about 10 eV, as seen in figure 1,

Also revealed are the signatures of multiple Rydberg resonance series that are superimposed on the smooth background cross section (figure 1). Beginning from threshold to higher photon energies, there first appears to be weak Rydberg series $2s^2 2p^2(^1D)nl$, converging to the first excited $O^{2+*}[2s^2 2p^2(^1D)]$ threshold at 51.25 eV, that can autoionize to the $O^{2+*}[2s^2 2p^2(^3P)] + e^-$ second continuum; whether this is a single series or several corresponding to different values of l is not entirely clear. Above the first excited threshold, a second series of resonances emerges, accumulating to the $O^{2+*}[2s^2 2p^2(^1S)]$ threshold at 54.09 eV. This next series, converging to the $O^{2+*}[(2s2p^3)(^5S)]$ threshold at 56.22 eV, seems to be perturbed by the lower members of a higher-lying

Rydberg series. Proceeding above this threshold, the most prominent Rydberg series is seen converging to the $O^{2+*}[(2s2p^3)(^3D)]$ threshold at 63.62 eV, with no discernible perturbation from the next highest, weak series. The lowest, strong ($n = 3$) resonance of this series at 58.32 eV lies 4.03 eV below the 63.62 eV threshold, and by using a quantum defect description (in eV)

$$\Delta E = 4.03 = 13.606/(3 - \mu)^2, \tag{9}$$

a quantum defect of $\mu = 1.2$ is revealed, which suggests this is the $[(2s2p^3)(^3D)]\,3p$ resonance.

As demonstrated in figure 1, the rather linear direct double ionization cross section is enhanced by fairly well-defined Feshbach resonance series. In contrast, the RMPS cross section in figure 3 shows somewhat oscillatory background and more randomly positioned jitter. By comparing the two results—experimental and theoretical—in figure 5, it is seen that, while the RMPS calculations reproduce the overall magnitude and general behavior of the experimental cross section, there is noticeable oscillation of the RMPS background about the smoother experimental background. This is associated with the rather coarse $3 \leqslant n \leqslant 10$ pseudostate representation of the second continuum contributing to the direct double photoionization cross section. Given that the second-electron continuum orbital is poorly spanned, it also follows that the infinite series of Rydberg resonance orbitals $3 \leqslant nl < \infty$ will be insufficiently represented by this $3 \leqslant n \leqslant 10$ pseudostate basis. As a result, even after factoring for the unphysical, slow oscillations of the RMPS background, the RMPS resonances do not seem to align with the experimental resonances that well, and, indeed, do not show the clear Rydberg series accumulations to well-defined thresholds. It should also be noted that the lowest-lying O^{+*} autoionizing Feshbach resonances, such as the $(1s^2 2s^2 2p^2(^1D))3l$ doubly-excited states, have resonance energy positions that are most uncertain, from a theoretical standpoint, and the detailed RMPS resonance structure is affected even more.

It is also clear from figure 5 that above about 62 eV, experiment and theory part ways. This occurs for the same reasons that were discussed in connection to the He case shown in figure 4. The orbital basis size used in the RMPS calculation for the double photoionization of atomic oxygen is simply too small to meaningfully cover the region of the double photoionization spectrum above 62 eV. And, even without resorting to comparison with experiment, the abrupt change in the overall slope of the cross section above 62 eV indicates that something is wrong here.

6. Summary

New experimental results for the double photoionization of atomic O are presented, with accompanying RMPS calculations, revealing prominent resonance structures. These Feshbach resonances are attributed to photoionized-excited intermediate states of the $O^{2+*}nl + e_1^-$ type, autoionizing to the doubly-photoionized $O^{2+} + e_2^- + e_1^-$ continua. The experimental cross section also demonstrates a Wannier nearly-linear threshold behavior for about 10 eV above threshold. The RMPS calculations involved orders of magnitude more channels than the simpler two-electron systems studied in the past, and thus were limited to a small $3 \leqslant n \leqslant 10$ pseudoorbital basis to represent each channel's second-electron continuum orbital, whether continuum ϵl or valence nl ($3 \leqslant n < -$). While the general magnitude and behavior of the RMPS cross section were similar to experiment, the limited basis representation led to unconverged, oscillatory behavior of the RMPS direct double continuum cross section, and erratic pseudoresonance approximations to the actual, infinite number of resonance contributions. A much larger basis set and computational effort would certainly reduce the present RMPS inaccuracies, and could help further explain the complicated Rydberg resonance spectra revealed in the new, highly-resolved experiment.

Acknowledgments

This work was supported in part by NASA APRA award NNX17AD41G (TWG) and the US Department of Energy, Office of Basic Sciences, Division of Chemical Science, Geosciences and Biosciences under Grant No. DE-FG02-03ER15428 (STM). This research used resources of the Advanced Light Source, a U.S. DOE Office of Science User Facility under contract no. DE-AC02-05CH11231.

Data availability statement

The data that support the findings of this study are available upon reasonable request from the authors.

ORCID iDs

T W Gorczyca https://orcid.org/0000-0003-4117-5790
S T Manson https://orcid.org/0000-0002-7072-4122

References

[1] McGuire J H, Berrah N, Bartlett R J, Samson J A R, Tanis J A, Cocke C L and Schlachter A S 1995 The ratio of cross sections for double to single ionization of helium by high energy photons and charged particles *Journal of Physics B Atomic Molecular Physics* **28** 913–40
[2] Bray I, Fursa D V, Kadyrov A S, Stelbovics A T, Kheifets A S and Mukhamedzhanov A M 2012 Electron- and photon-impact atomic ionisation *Phys. Reports* **520** 135–74
[3] Burke P G 2011 *R-matrix Theory of Atomic Collisions* (New York: Springer)
[4] Gorczyca T W, Lee T-G and Pindzola M S 2013 Two-electron photoionization processes in He@C_{60} using the R-matrix with pseudostates and time-dependent close-coupling methods *Journal of Physics B Atomic Molecular Physics* **46** 195201
[5] Griffin D C, Pindzola M S, Ballance C P and Colgan J 2009 Double photoionization of Be and Mg atoms using the R -matrix-with-pseudostates method *Phys. Rev.* A **79** 023413
[6] Colgan J, Griffin D C, Ballance C P and Pindzola M S 2009 Total cross sections for the double photoionization of Li from the ground and excited states *Phys. Rev.* A **80** 063414
[7] Griffin D C, Ballance C P and Pindzola M S 2009 Nonperturbative calculations of double photoionization of Ne: An R matrix with pseudostate-convergence study *Phys. Rev.* A **80** 023420
[8] Carter S L and Kelly H P 1977 Double photoionization of neon and argon *Phys. Rev.* A **16** 1525–34
[9] Pan C and Kelly H P 1989 Photoionization cross sections of the ar atom for production of singly and doubly charged ions near the 2p threshold *Phys. Rev.* A **39** 6232–40
[10] García J, Ramírez J M, Kallman T R, Witthoeft M, Bautista M A, Mendoza C, Palmeri P and Quinet P 2011 Modeling the Oxygen K Absorption in the Interstellar Medium: An XMM-Newton View of Sco X-1. *Astrophys. Journal Letters* **731** L15
[11] Stolte W C, Lu Y, Samson J A R, Hemmers O, Hansen D L, Whitfield S B, Wang H, Glans P and Lindle D W 1997 The K-shell Auger decay of atomic oxygen *Journal of Physics B Atomic Molecular Physics* **30** 4489–97
[12] McLaughlin B M, Ballance C P, Bowen K P, Gardenghi D J and Stolte W C 2013 High Precision K-shell Photoabsorption Cross Sections for Atomic Oxygen: Experiment and Theory *Astrophys. Journal* **771** L8
[13] Angel G C and Samson J A R 1988 Total photoionization cross sections of atomic oxygen from threshold to 44.3 A *Phys. Rev.* A **38** 5578–85
[14] He Z X, Moberg R and Samson J A R 1995 Threshold behavior in single-photon double ionization of atomic oxygen *Phys. Rev.* A **52** 4595–8
[15] Feshbach H 1958 Unified theory of nuclear reactions *Ann. Phys.* **5** 357–90
[16] Svensson S, Eriksson B, Martensson N, Wendin G and Gelius U 1988 Electron shake-up and correlation satellites and continuum shake-off distributions in x-ray photoelectron spectra of the rare gas atoms *J. Electron. Spectrosc. Relat. Phenom.* **47** 327–84
[17] Becker U, Hemmers O, Langer B, Lee I, Menzel A, Wehlitz R and Amusia M Y 1993 Multiplet-changing auger transitions in valence double photoionization *Phys. Rev.* A **47** R767–70
[18] Wehlitz R, Huang M-T, Berrington K A, Nakazaki S and Azuma Y 1999 One-step double autoionization into the double-photoionization continuum *Phys. Rev.* A **60** R17–20
[19] Samson J A R and Pareek P N 1985 Absolute photoionization cross sections of atomic oxygen *Phys. Rev.* A **31** 1470–6
[20] Stolte W C, Guillemin R, Yu S-W and Lindle D W 2008 Photofragmentation of HCl near the chlorine $L_{2,3}$ ionization threshold: new evidence of a strong ultrafast dissociation channel *Journal of Physics B Atomic Molecular Physics* **41** 145102
[21] Stolte W C, Guillemin R, Demchenko I N, Öhrwall G, Yu S-W, Young J A, Taupin M, Hemmers O, Piancastelli M N and Lindle D W 2010 Inner-shell photofragmentation of Cl_2 *Journal of Physics B Atomic Molecular Physics* **43** 155202
[22] Domke M, Xue C, Puschmann A, Mandel T, Hudson E, Shirley D A, Kaindl G, Greene C H, Sadeghpour H R and Petersen H 1991 Extensive double-excitation states in atomic helium *Phys. Rev. Lett.* **66** 1306–9
[23] King G C, Tronc M, Read F H and Bradford R C 1977 An investigation of the structure near the $L_{2,3}$ edges of argon, the $M_{4,5}$ edges of krypton and the $N_{4,5}$ edges of xenon, using electron impact with high resolution *Journal of Physics B Atomic Molecular Physics* **10** 2479–95
[24] Gullikson E M, Korde R, Canfield L R and Vest R E 1996 Stable silicon photodiodes for absolute intensity measurments in the vuv and soft x-ray regions *J. Electron. Spectrosc. Relat. Phenom.* **80** 313–6
[25] Berkowitz J 2002 *Atomic and Molecular Photoabsorption: Absolute Total Cross Sections* (New York: Academic)
[26] Berkowitz J 2015 *Atomic and Molecular Photoabsorption: Absolute Partial Cross Sections* (New York: Academic)
[27] Ralchenko Y, Kramida A E, Reader J and Nist ASD Team 2011 *Nist atomic spectra database (ver. 4.1.0)* (National Institute of Standards and Technology) (http://physics.Nist.gov/asd)
[28] Ressler T 2009 (http://www.winxas.de/)
[29] Meyer K W and Greene C H 1994 Double photoionization of helium using R-matrix methods *Phys. Rev.* A **50** 3573
[30] Marchalant P J and Bartschat K 1997 R matrix with pseudostates calculation for single and double ionization of helium by photon impact *Phys. Rev.* A **56** 1697
[31] Gorczyca T W and Badnell N R 1997 Photoionization—excitation of helium using an R-matrix with pseudostates method *Journal of Physics B Atomic Molecular Physics* **30** 3897–911
[32] https://wiki.hpcc.msu.edu/
[33] Froese Fischer C 1991 A general multi-configuration Hartree-Fock program *Comput. Phys. Commun.* **64** 431–54
[34] Badnell N R and Breit-Pauli A 2011 A Breit-Pauli distorted wave implementation for AUTOSTRUCTURE *Comput. Phys. Commun.* **182** 1528–35
[35] Wehlitz R *et al* 1997 LETTER TO THE EDITOR: Photon energy dependence of ionization-excitation in helium at medium energies *Journal of Physics B Atomic Molecular Physics* **30** L51–8
[36] Wannier G H 1953 The Threshold Law for Single Ionization of Atoms or Ions by Electrons *Phys. Rev.* **90** 817–25